Proceedings of the 7th International Symposium on Cavitation
CAV2009 - Paper No. 21
August 17-22, 2009, Ann Arbor, Michigan, USA

Supercavitating motion of a wedge in a jet

Y.A. Antipov, A.Y. Zemlyanova
Department of Mathematics, Louisiana State University
Baton Rouge LA 70803, U.S.A.

Abstract

The problem of determining the free surface of a jet incident on a rigid wedge and the boundary of a cavity behind the wedge is considered. The single- and double-spiral-vortex models by Tulin are used to describe the flow at the rear part of the cavity. The location of the wedge in the jet and the sides lengths are arbitrary. This circumstance makes the flow domain doubly connected for the single-vortex model whilst it is simple connected for the double-vortex model. Both the models are solved in closed form by the method of conformal mappings. The maps are expressed through the solutions to certain Riemann-Hilbert problems. For the former model, this problem is formulated on a genus-1 Riemann surface. The double-vortex model requires the solution to a standard Riemann-Hilbert problem on a plane. It is found that the drag and lift are practically the same whilst the jet surface, the cavity boundary at the rear part and the deflection angle of the jet at infinity are different. Also, the problem of determining the parameters for the conformal mapping in the single-vortex model has two solutions. It is shown that one of the solutions leads to a non-physical shape of the cavity and needs to be discarded. The case of a wedge in a channel with a free surface is also analyzed.

1 Introduction

The flow induced by the supercavitating motion of a strut is of considerable interest in many marine applications including the design and analysis of hydrofoils and marine propellers. It is a relatively easy matter to solve a problem of two-dimensional, irrotational, incompressible, steady flow past a polygonal obstacle with rigid walls when the flow domain is simply connected and its boundary is prescribed. It is more difficult to deal with nonsymmetric flow when the boundary of the flow domain is free and the model assumes the existence of a cavity behind the body. Since flow is unsteady at the rear part of the cavity, any steady-state model of supercavitating flow is approximate. The most successful steady-state cavity closure models achieve a reasonable balance between the mathematical rigorousness and

experimental observations and allow to apply the theory of functions of a complex variable and derive an analytical solution.

The models of supercavitating flow used in the literature are described in [8], [14], [9], [6]. These models include the Joukowsky open wake model, the Riabouchinsky image model, the Efros-Gilbarg-Rock-Kreisel re-entrant jet model, and the two spiral-vortex models by Tulin [13]. The open wake model assumes the existence of a semi-infinite wake behind the obstacle. Riaboushinsky proposed to place an image obstacle downstream of the real body. In the re-entrant jet model, the flow domain is a two-sheeted Riemann surface formed by gluing two replicas of the physical plane along the hydrofoil. It is assumed that a part of the main stream reverses the direction and proceeds to the second sheet through the junction line of the Riemann surface.

In the Tulin spiral-vortex models, there are two vortices in the rear part of the cavity. The single-spiral-vortex model assumes that the velocity is continuous at the centers of the vortices but the two branches which form the cavity boundary are discontinuous at the physical plane (the flow can be considered on an infinitely-sheeted Riemann surface of a logarithmic function whose branch points are the centers of the vortices). In the double-spiral-vortex model, the speed is discontinuous at the vortices and there is a semi-infinite wake behind the cavity. The speed on the wake boundary is constant and is the same as at infinity. From the mathematical point of view, there are two features which distinguish these two models. First, the complex velocity potential, w, has different asymptotics at the centers, C_j, of the vortices. For the single-spiral-vortex model, $\ln dw/dz = O\{[w - w(C_j)]^{-1/2}\}$, and for the double-spiral-vortex model, $\ln dw/dz = O\{\ln[w - w(C_j)]\}$, $z \to C_j$. Another difference is that for the former model, apart from some particular cases, the flow domain is multiply connected. In the second model, the flow domain is always simply-connected. The double-spiral-vortex model was used for the analysis of a cavitating foil beneath a free surface [10], in the case of a cavitating polygonal plate in a plane [5], and in a numerical scheme for the a cavitating foil of arbitrary shape [7]. For the simply-connected case, the nonlinear single-spiral-vortex model was employed [11], [12], [9]. The same model and the method of Riemann surfaces were used in [1], [2] for the case of two foils in a channel, and a wedge with a trailing and a partial cavity in a plane. A method of the Riemann-Hilbert problem for piece-wise automorphic functions for supercavitating flow in an $n+1$-connected flow domain was proposed in [3] . We emphasize that in these papers, the numerical computations were implemented for the simply connected case only. Recently [4], the single-spiral-vortex model was applied to solve analytically the problem of supercavitating flow of a wedge beneath a free surface. The work presented herein is intended as a comparative study of the single- and double-spiral-vortex models applied to supercavitating jet flow past a wedge when the location and the side lengths of the wedge are arbitrary.

2 Double-spiral-vortex model

The flow is two-dimensional, incompressible, irrotational, and the gravity is neglected. The vertex, A, of the wedge, DAB, is fixed and is chosen to be the origin of the plane $z = x_1 + ix_2$ (figure 1). Far away from the wedge, as $x_1 \to -\infty$, the upper and the lower free surfaces of the jet are described by the equations $x_2 = h_1$ and

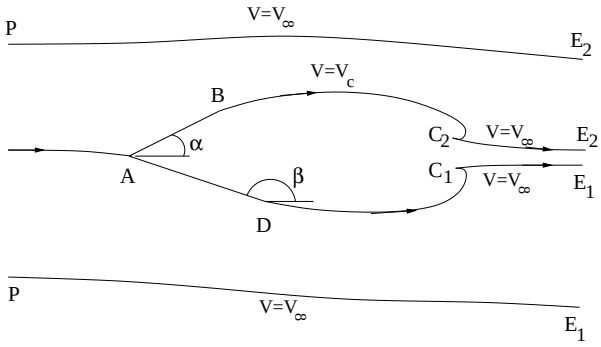

Figure 1: The double-spiral-vortex model domain.

$x_2 = -h+h_1$, respectively. As $x_1 \to -\infty$, the velocity of the flow is also prescribed, $\mathbf{v} = (V_\infty, 0)$. The upper and the lower sides of the wedge have lengths λ_1 and λ_2 and form the angles α_0 and β_0 with the x_1-axis, respectively. A motion with the following features is to be considered:

(1) The wedge may move about the x_3-axis orthogonal to the flow plane. The angle of yaw, δ, is to be determined from the condition that the vertex A is the only stagnation point of the flow.

(2) The sides of the wedge are straight and rigid. The flow branches at the point A, and the velocity vector is tangent to the faces of the wedge,

$$\arg \frac{dw}{dz} = \begin{cases} -\alpha, & z \in AB, \\ \pi - \beta, & z \in AD, \end{cases} \tag{2.1}$$

where $\alpha = \alpha_0 + \delta$ and $\beta = \beta_0 + \delta$. These two angles define the actual position of the wedge when the flow becomes steady-state. The derivative $\overline{dw/dz} = v_1 + iv_2$ is the complex velocity, v_1 and v_2 are the components of the velocity vector $\mathbf{v}$, and $w(z) = \phi(z) + i\psi(z)$ is a complex potential of the flow.

(3) Behind the wedge, there is a cavity formed by two branches ABC_2 and ADC_1 of the same streamline. The cavity pressure, p_c, is constant and prescribed. The flow separates smoothly from the points B and D. The free streamlines ABC_2 and ADC_1 form two spirals at the ending points C_2 and C_1. The speed on the boundary of the cavity is constant, $V = V_c$, where $V_c = \sqrt{\sigma+1}V_\infty$, σ is the cavitation number, $\sigma = 2(p_\infty - p_c)(\rho V_\infty^2)^{-1}$, ρ is the density of the liquid, and p_∞ is the pressure as $x_1 \to -\infty$. At the centers of the spiral vortices, C_1 and C_2, the logarithm of the complex velocity has the following singularity [13]:

$$\ln \frac{dw}{dz} = O\{\ln[w - w(C_j)]\}, \quad z \to C_j, \quad j = 1, 2. \tag{2.2}$$

At the points C_j, the speed is discontinuous. First, the streamlines spiral at speed V_c, then the speed jumps to $V = V_\infty$, and the streamlines spiral backwards and continue in the direction of the infinite point $+\infty + ix_2$ (x_2 is finite) forming a wake. Thus, we have

$$\left|\frac{dw}{dz}\right| = \begin{cases} V_c, & z \in BC_2 \cup DC_1, \\ V_\infty, & z \in C_2E_2 \cup C_1E_1, \end{cases}$$

$$\operatorname{Im} w(z) = \psi_0, \quad z \in ABC_2E_2 \cup ADC_1E_1, \tag{2.3}$$

where $\psi_0 = \text{const}$.

(4) The boundary of the free surfaces of the jet is formed by two streamlines, PE_2 and PE_1, and the speed on the free surfaces is assumed to be constant $V = V_\infty$. Thus,

$$\left|\frac{dw}{dz}\right| = V_\infty, \quad z \in PE_1 \cup PE_2,$$

$$\operatorname{Im} w(z) = \begin{cases} -\psi_1, & z \in PE_1, \\ \psi_2, & z \in PE_2, \end{cases} \tag{2.4}$$

where ψ_1 and ψ_2 are constants.

(5) The complex potential $w(z)$ has the same values at the centers of the double spirals, the

points C_1 and C_2. Since these two points lie on the two branches of the same streamline, this assumption is equivalent to the following real condition:

$$\operatorname{Re} w(C_1) = \operatorname{Re} w(C_2). \tag{2.5}$$

(6) The width of the jet is finite as $x_1 \to +\infty$. This condition means that

$$\arg \frac{dw}{dz}\bigg|_{z=E_1} = \arg \frac{dw}{dz}\bigg|_{z=E_2}. \tag{2.6}$$

The double-spiral-vortex model of supercavitating flow of a jet past n finite obstacles is flow in a simply connected domain regardless of the number n. Therefore, there exists a function $z = f(\zeta)$ which maps conformally a half-plane into the flow domain. We denote the preimages of the points A, B, C_j, D, E_j, and P by a, b, c_j, d, e_j, and p, respectively. Three real parameters can be fixed arbitrarily, and we choose $a = 0$, $d = -1$, and $p = \infty$.

To derive the expression of the mapping function $f(\zeta)$, we represent its derivative in the form

$$\frac{df}{d\zeta} = \frac{\omega_0(\zeta)}{V_\infty} e^{-\omega_1(\zeta)}, \tag{2.7}$$

where

$$\omega_0(\zeta) = \frac{dw}{d\zeta}, \quad \omega_1(\zeta) = \ln \frac{dw}{V_\infty dz}. \tag{2.8}$$

The standard Schwarz-Christoffel formula is employed to recover the function $\omega_0(\zeta)$,

$$\omega_0(\zeta) = \frac{q_1 \zeta}{(\zeta - e_1)(\zeta - e_2)}. \tag{2.9}$$

By integrating this expression, we find the complex potential $w(z(\zeta))$

$$w = \frac{q_1}{e_1 - e_2} \left[e_1 \ln(\zeta - e_1) - e_2 \ln(\zeta - e_2) \right] + q_2. \tag{2.10}$$

Here $\ln(\zeta - e_j)$ are the branches fixed by the condition $0 \le \arg(\zeta - e_j) < \pi$, and q_1 and q_2 are some constants. To fix these constants, in addition to the parametric ζ-plane, consider the w-plane. Since $w(0) = 0$ we may find q_2,

$$q_2 = -\frac{q_1}{e_1 - e_2} \left[e_1 \ln(-e_1) - e_2(\ln e_2 + i\pi) \right]. \tag{2.11}$$

Determine now the constant q_1. Notice that as a point ζ traverses around the point $\zeta = e_j$ $(j = 1, 2)$ along a path in the upper half-plane, the variation of the function $\ln(\zeta - e_j)$ is $i\pi$ whilst the corresponding variation of w is $-i\psi_j$. Consequently, $q_1 = -(\psi_1 + \psi_2)/\pi$, $e_1 = -\psi_1 e_2/\psi_2$. The use of the conservation of mass law defines the constants ψ_1 and ψ_2

$$\psi_1 = V_\infty(h - h_1), \quad \psi_2 = V_\infty h_1. \tag{2.12}$$

Thus, the function $\omega_0(\zeta)$ is defined by the expression

$$\omega_0(\zeta) = -\frac{V_\infty h \zeta}{\pi[\zeta - (1 - h/h_1)e_2](\zeta - e_2)} \tag{2.13}$$

which possesses one unknown real parameter e_2.

We turn now to the determination of the function $\omega_1(\zeta)$. On referring to the boundary conditions (2.1), (2.3), and (2.4), we see from (2.8) that

$$\begin{gathered} \operatorname{Re} \omega_1(\xi) = 0, \quad \xi \in pe_1 \cup e_1c_1 \cup c_2e_2 \cup e_2p, \\ \operatorname{Re} \omega_1(\xi) = \frac{1}{2} \ln(1 + \sigma), \quad \xi \in c_1d \cup bc_2, \\ \operatorname{Im} \omega_1(\xi) = -\alpha, \quad \xi \in ab, \\ \operatorname{Im} \omega_1(\xi) = \pi - \beta, \quad \xi \in da. \end{gathered} \tag{2.14}$$

The function $\omega_1(\zeta)$ can be found in terms of singular integrals by solving a Riemann-Hilbert

problem associated with the problem (2.14). By evaluating the singular integrals we have

$$\omega_1(\zeta) = \frac{i\ln(1+\sigma)}{2\pi}\left(\ln\frac{\rho_1-\hat{\zeta}}{\rho_1+\hat{\zeta}} - \ln\frac{\rho_2-1/\hat{\zeta}}{\rho_2+1/\hat{\zeta}}\right)$$

$$-i\alpha + \frac{\pi+\alpha-\beta}{\pi}\ln\frac{\sqrt{b}+i\hat{\zeta}}{\sqrt{b}-i\hat{\zeta}}. \qquad (2.15)$$

Here

$$\hat{\zeta} = \sqrt{\frac{\zeta-b}{\zeta+1}}, \quad \rho_1 = \sqrt{\frac{b-c_1}{-c_1-1}}, \quad \rho_2 = \sqrt{\frac{c_2+1}{c_2-b}},$$

$$\arg(\rho_1\pm\hat{\zeta}),\ \arg(\rho_2\pm 1/\hat{\zeta}),\ \arg(\sqrt{b}\pm i\hat{\zeta}) \in [-\pi,\pi], \qquad (2.16)$$

$\rho_j > 0$ $(j = 1, 2)$, and the single branch of the function $\hat{\zeta}$ has the following boundary values as $\zeta = \xi \pm i0$:

$$\hat{\zeta} = \begin{cases} |\hat{\zeta}|, & \xi < -1 \text{ or } \xi > b, \\ \pm i|\hat{\zeta}|, & -1 < \xi < b. \end{cases} \qquad (2.17)$$

The solution has to vanish at the point p. This requirement leads to the following real condition for the unknown parameters of the mapping

$$-\ln(1+\sigma)\ln\frac{2\chi^+(c_2)+2c_2-b+1}{-2\chi^+(c_1)-2c_1+b-1}$$

$$+2\alpha\rho^- - 2(\pi-\beta)\rho^+ = 0, \qquad (2.18)$$

where

$$\rho^\pm = \frac{\pi}{2} \pm \sin^{-1}\frac{1-b}{1+b}. \qquad (2.19)$$

The derivative of the conformal mapping (2.7) has been expressed through the functions $\omega_0(\zeta)$ and $\omega_1(\zeta) = i\Phi(\zeta)$, $\operatorname{Im}\zeta > 0$, given by (2.13) and (2.15). It will be convenient to rewrite its expression in the form

$$\frac{df}{d\zeta} = hF(\zeta), \quad F(\zeta) = -\frac{\zeta e^{-\omega_1(\zeta)}}{\pi(\zeta-e_1)(\zeta-e_2)}. \qquad (2.20)$$

The function $F(\zeta)$ has 5 unknown real parameters, e_2, c_1, c_2, and b, the preimages of the points E_2, C_1, C_2, and B, and the yaw angle δ. The parameter e_1 is expressed through the unknown e_2 by

$$e_1 = \frac{l-1}{l}e_2, \quad l = h_1/h \in (0,1). \qquad (2.21)$$

For the definition of these five parameters, we have the condition (2.18), the following two geometric conditions:

$$\operatorname{Im}\int_0^b F(\zeta)d\zeta = \lambda_1^\circ \sin\alpha,$$

$$\operatorname{Im}\int_{-1}^0 F(\zeta)d\zeta = \lambda_2^\circ \sin\beta, \qquad (2.22)$$

and the relations

$$\ln\frac{c_1-e_1}{c_2-e_1} = \frac{e_2}{e_1}\ln\frac{e_2-c_1}{e_2-c_2},$$

$$\operatorname{Im}\omega_1(e_1) = \operatorname{Im}\omega_1(e_2). \qquad (2.23)$$

Here $\lambda_j^\circ = \frac{\lambda_j}{h}$. The last two conditions follow from equations (2.5) and (2.6) of the model. Notice that equation (2.18) and the second equation in (2.23) are linear with respect the parameter δ. This makes it possible to express this parameter from one of these two equations say, (2.18), through the other four parameters, b, c_1, c_2, and e_2. For the solution of the system of the four nonlinear equations (2.22) and (2.23) we use a scheme based on the Newton iterative method [4].

Since the derivative of the conformal mapping has been found, it is possible to reconstruct the free boundary which consists of the jet surface, the cavity and the wake profile. By integrating

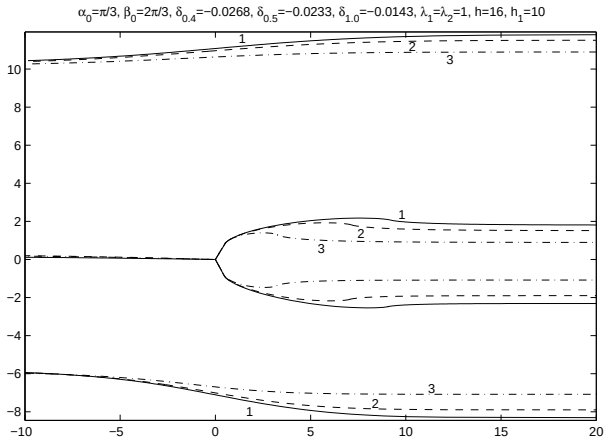

Figure 2: The cavity, wake, and jet profiles when $\lambda_1 = \lambda_2 = 1$, $h = 16$, $h_1 = 10$, $\alpha_0 = \frac{\pi}{3}$, and $\beta_0 = \frac{2\pi}{3}$ for some values of the cavitation parameter σ: $\sigma = 0.4$ (1), $\sigma = 0.5$ (2), and $\sigma = 1$ (3).

the function $df/d\zeta$, we obtain the lower and upper boundaries of the jet,

$$z(\tau) = D + \int\limits_{d\tau} \frac{df}{d\zeta} d\zeta, \quad \tau \in pe_1 \ (z \in PE_1),$$

$$z(\tau) = B + \int\limits_{b\tau} \frac{df}{d\zeta} d\zeta, \quad \tau \in pe_2 \ (z \in PE_2). \quad (2.24)$$

For the cavity and wake boundaries, we have similar formulas. For the lower part of the cavity boundary $\tau \in dc_1$ ($z \in DC_1$) and for the upper one, $\tau \in bc_2$ ($z \in BC_2$). Figure 2 shows the cavity shape and the profile of the wake and the jet when $\lambda_1^\circ = \lambda_2^\circ = 0.1$, $l = \frac{5}{8}$, and $\alpha_0 = \pi - \beta_0 = \frac{\pi}{3}$ for the values 0.4, 0.5, and 1 of the cavitation number σ. The parameters of the conformal mapping for $\sigma = 1$ have the following values: $e_1 = -1.82018$, $c_1 = -1.74692$, $b = 1.18188$, $c_2 = 2.62667$, and $e_2 = 3.03363$. It is seen that the cavity size and the width of the wake behind the cavity increase when the the cavitation number decreases.

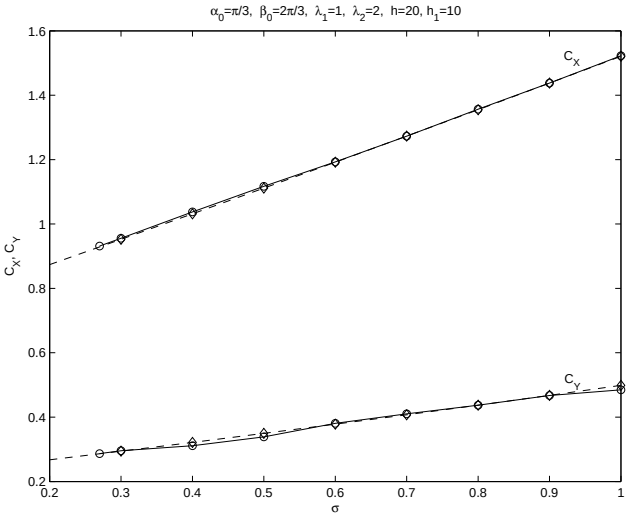

Figure 3: The drag and lift coefficients, C_X and C_Y, when $\lambda_1 = 1$, $\lambda_2 = 2$, $h = 20$, $h_1 = 10$, $\alpha_0 = \pi - \beta_0 = \frac{\pi}{3}$ vs the parameter σ: the single-spiral-vortex model (–) and the double-spiral-vortex model (- -).

We proceed now to compute the drag and lift coefficients

$$C_X + iC_Y = \frac{2(X + iY)}{\rho V_\infty^2 \lambda^\circ h}, \quad (2.25)$$

where $\lambda^\circ = \lambda_1^\circ \sin\alpha + \lambda_2^\circ \sin\beta$, X and Y are drag and lift, respectively, which by Bernoulli's law can be represented in the form

$$X + iY = -\frac{i\rho}{2} \int\limits_{DAB} (V_c^2 - V^2) dz, \quad (2.26)$$

where $V = |dw/dz|$. We have finally

$$C_X + iC_Y = -\frac{i}{\lambda^\circ} \int\limits_{dab} [\sigma + 1 - e^{2\,\mathrm{Re}\,\omega_1(\zeta)}] F(\zeta) d\zeta. \quad (2.27)$$

For the parameters $\alpha_0 = \pi - \beta_0 = \frac{\pi}{3}$, $\lambda_1^\circ = 0.05$, $\lambda_2^\circ = 0.1$ and $l = 0.5$, the drag and lift coefficients

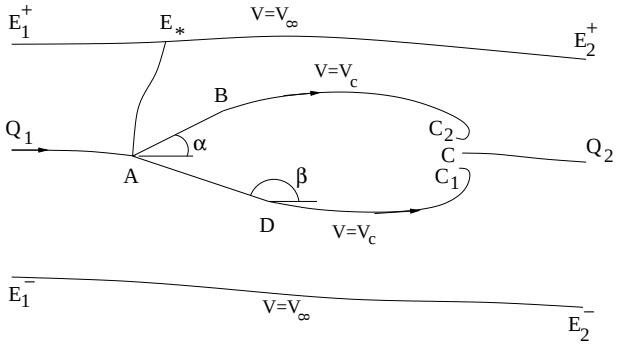

Figure 4: The single-spiral-vortex model domain $\tilde{\mathcal{D}}$.

increase when the cavitation number σ increases (figure 3).

Our scheme applied to a single hydrofoil for small $l = h_1/h$ is consistent with the results by [10] for the coefficient

$$C_D + iC_L = \frac{\lambda^\circ}{\lambda_1^\circ + \lambda_2^\circ}(C_X + iC_Y) \qquad (2.28)$$

obtained for a foil beneath a free surface ($h_1 = 1$, $h = \infty$). For $h = 1000$ and $h_1 = 1$, the angle of attack 5.66° and $\sigma = 0.096$, the coefficient $C_D + iC_L$ obtained from our jet-solution is $1.900367 \cdot 10^{-2} + i \cdot 0.191522$, and the one reported in [10] is $0.019 + i0.191$.

3 Single-spiral-vortex model

The first two assumptions, (1) and (2), of the single-spiral-vortex model are the same as for the double-spiral-vortex model described in Section 2. We write down the other assumptions of the model which distinguish this model from the double-spiral-vortex model.

(3) The closure cavity mechanism for the single-spiral-vortex model is different from (2.2) and is described by [13], [2]

$$\log \frac{dw}{dz} \sim -K((w - w(C))^{-1/2}), \quad z \to C. \qquad (3.29)$$

Here $-\pi \le \arg[w(z) - w(C)] \le \pi$, K is a positive constant, and the branch of the square root is chosen such that $[w(z) - w(C)]^{1/2} > 0$ when $\arg[w(z) - w(C)] = 0$. The two branches of the dividing streamline at the centers of the vortices behind the foil, C_1 and C_2, pass to a half of an infinitely sheeted Riemann surface of the logarithmic function with the branch points C_1 and C_2. After that the same streamline emerges from the infinite sheet of the Riemann surface and returns to a point C of the first, physical, sheet. In contrast to the double-spiral-vortex model, the speed is continuous at the rear part of the cavity (figure 4).

On the boundary of the cavity, the complex potential $w(z)$ satisfies the following boundary conditions:

$$\operatorname{Im} w(z) = K_0, \quad z \in L_1,$$

$$\left|\frac{dw}{dz}\right| = \begin{cases} V_\infty, & z \in L_0, \\ V_c, & z \in BC^+ \cup DC^-, \end{cases} \qquad (3.30)$$

where K_0 is a real constant, and the contour L_1 consists of the boundary of the cavity $BC_2 \cup DC_1$ and the faces of the wedge DAB.

(4) On the jet surface $L_0 = E_1^- E_2^- \cup E_1^+ E_2^+$,

$$\operatorname{Im} w(z) = K_1^\pm, \quad z \in E_1^\pm E_2^\pm, \qquad (3.31)$$

where K_1^+ and K_1^- are some real constants.

(5) By contrast with the double-spiral-vortex model, the flow domain, $\tilde{\mathcal{D}}$, is not simply connected but doubly connected. To assure that the flow is single-valued, it is required that

$$\int_{L_*} dz = 0, \qquad (3.32)$$

Here L_* is a closed contour in the flow domain exterior to the contour L_1.

As for the double-spiral-vortex model, we use the conformal mapping technique. Let $z = f(\zeta)$ map the exterior of two cuts, $l_1 = [0, 1]$ and $l_0 = [m, \infty)$ onto the physical domain $\tilde{D}$. Here $m \in (1, +\infty)$ is a parameter to be fixed. Denote the preimages of the points A, B, C, D, $E_1^{\pm}$, and $E_2^{\pm}$ by a, b, c, d, e_1, and e_2, respectively. Since such a map is defined up to one real parameter and since $e_1 \neq e_2$, we choose $e_1 = \bar{e}_2$. Clearly, two cases need to be considered, $e_1 = e_0 + i0$ and $e_1 = e_0 - i0$, where $e_0 = |e_1| = |e_2|$, $e_0 \in (m, +\infty)$.

As before, the derivative $df/d\zeta$ is conveniently represented in terms of two functions, $\omega_0(\zeta)$ and $\omega_1(\zeta)$, by (2.7).

The function $\omega_0(\zeta)$ is analytic in the exterior of the cuts l_0 and l_1. At infinity, the function $f(\zeta)$ decays as $\tilde{K}\zeta^{-1/2}$, $\tilde{K} = \text{const}$. This implies $\omega_0(\zeta) = O(\zeta^{-3/2})$, $\zeta \to \infty$. At the preimages of the points $E_j^{\pm}$, it has a logarithmic singularity, $f(\zeta) \sim h\pi^{-1}(-1)^{j-1}\ln(\zeta - e_0)$, $j = 1, 2$. Since $dw/dz \sim V_\infty$, $\zeta \to e_1$, we obtain $\omega_0(\zeta) \sim hV_\infty[\pi(\zeta - e_0)]^{-1}$, $\zeta \to e_1$. It has been shown in [2] that the function $dw/d\zeta$ has to vanish at the stagnation point and the point where the branched streamline emerges from the Riemann surface of flow. In our case this means that $\omega_0(\zeta)$ has simple zeros at the points a and c. Because of the first condition in (3.30) and equation (3.31), $\operatorname{Im}\omega_0(\zeta) = 0$ on l_0 and l_1. All these conditions can be written as a homogeneous Riemann-Hilbert problem. By solving it we find that $a = \bar{c}$. Without loss of generality, we assume that $a \in l_1^+$ and then $c \in l_1^-$. The most general form of the function $\omega_0(\zeta)$ with such properties is

$$\omega_0(\zeta) = hV_\infty\omega_0^*(\zeta), \tag{3.33}$$

where

$$\omega_0^*(\zeta) = \frac{p^{1/2}(e_1)}{\pi p^{1/2}(\zeta)}\left(\frac{1}{\zeta - e_0} - \frac{1}{a - e_0}\right). \tag{3.34}$$

Here $p(\zeta) = \zeta(1 - \zeta)(\zeta - m)$ and $p^{1/2}(\zeta)$ is the branch fixed by the condition $p^{1/2}(\xi) > 0$ if $\xi < 0$. At the banks of the cuts l_0 and l_1, $\zeta = \xi \pm i0$, it has the properties $p^{1/2}(\zeta) = \mp i|p^{1/2}(\xi)|$, $0 < \xi < 1$, and $p^{1/2}(\zeta) = \pm i|p^{1/2}(\xi)|$, $m < \xi < +\infty$. If $1 < \xi < m$, then the function $p^{1/2}(\xi)$ is negative.

The function $\omega_0(\zeta)$ has three real parameters, a, e_0, and m to be determined. By conservation of mass, we can write down the first real condition for them,

$$\operatorname{Im}\int_a^{e_*}\omega_0(\zeta)d\zeta = h_1V_\infty, \tag{3.35}$$

where e_* is the preimage of a point E_* in the upper boundary of the jet. This condition can be transformed into the form

$$\operatorname{Im}\int_1^m\omega_0^*(\zeta)d\zeta = \begin{cases} l - 1, & e_1 \in l_0^-, \\ l, & e_1 \in l_0^+. \end{cases} \tag{3.36}$$

From the conditions (2.1) and (3.29) to (3.31) we conclude that the function $\omega_1(\zeta)$ satisfies the boundary conditions

$$\operatorname{Re}\omega_1(\zeta) = \begin{cases} \log\sqrt{\sigma + 1}, & \zeta \in bcd, \\ 0, & \zeta \in l_1, \end{cases}$$

$$\operatorname{Im}\omega_1(\zeta) = \begin{cases} -\alpha, & \zeta \in ab, \\ \pi - \beta, & \zeta \in da, \end{cases} \tag{3.37}$$

and as $\zeta \to c$, $\omega_1(\zeta) = O(1/(z - c))$. The function $\omega_1(\zeta)$ has a logarithmic singularity at the point a and it is bounded at the points b and d. At infinity, the function $\omega_1(\zeta)$ is bounded and it vanishes at the point $\zeta = e_1$.

Apart from the conditions at $\zeta = \infty$ and $\zeta = e_1$, these conditions are the same as those for the function $\omega_1(\zeta)$ in the double-spiral-vortex model for a wedge beneath a free surface [4]. Therefore, the function $\omega_1(\zeta)$ can be determined in a similar manner through the solution to a Riemann-Hilbert problem on a two-sheeted genus-1 Riemann surface, $\mathcal{R}$, of the algebraic function

$$u = \begin{cases} p^{1/2}(\zeta), & \zeta \in \mathbb{C}_1, \\ -p^{1/2}(\zeta), & \zeta \in \mathbb{C}_2. \end{cases} \tag{3.38}$$

Here $\mathbb{C}_1$ and $\mathbb{C}_2$ are two replicas of the extended ζ-plane with the cuts l_0 and l_1. We write down only the final formulas for the solution. Let $\Phi(\zeta, u) = -i\omega_1(\zeta)$ on the upper sheet $\mathbb{C}_1$ and $\Phi(\zeta, u) = i\,\overline{\omega_1(\bar{\zeta})}$ on the lower sheet $\mathbb{C}_2$. Then

$$\Phi(\zeta, u) = X(\zeta, u)[\Psi(\zeta, u) + \Omega(\zeta, u)], \quad (\zeta, u) \in \mathcal{R}, \tag{3.39}$$

where

$$\Psi(\zeta, u) = -\frac{\alpha}{2\pi i} \int\limits_{ab} \frac{(1 + u/v)d\xi}{X^+(\xi, v)(\xi - \zeta)} + \frac{\pi - \beta}{2\pi i} \int\limits_{da} \frac{(1 + u/v)d\xi}{X^+(\xi, v)(\xi - \zeta)} - \frac{\ln(\sigma + 1)}{4\pi} \int\limits_{bcd} \frac{(1 + u/v)d\xi}{X(\xi, v)(\xi - \zeta)}, \tag{3.40}$$

and $v = u(\xi)$. The function $\Omega(\zeta, u)$ is a rational function on the surface $\mathcal{R}$ given by

$$\Omega(\zeta, u) = iM_0 \frac{u(\zeta) + u(c)}{\zeta - c} + (M_1 + iM_2) \times \frac{u(\zeta) + u(\eta_0)}{\zeta - \eta_0} - (M_1 - iM_2) \frac{u(\zeta) - \overline{u(\eta_0)}}{\zeta - \bar{\eta}_0} + M_3, \tag{3.41}$$

where M_j $(j = 0, 1, 2, 3)$ are real constants to be fixed.

As for the function $X(\zeta, u)$, it is a piece-wise meromorphic function, symmetric on the surface, $X(\zeta, u) = \overline{X(\bar{\zeta}, -u(\bar{\zeta}))}$, $(\zeta, u) \in \mathcal{R} \setminus \mathcal{L}$, $\mathcal{L} = l_0 \cup l_1$, discontinuous through the contour $dab \in \mathcal{R}$, and whose one-sided limits satisfy the boundary condition

$$X^+(\xi, v) = -X^-(\xi, v), \quad (\xi, v) \in dab. \tag{3.42}$$

This function is defined by singular integrals

$$X(\zeta, u) = \exp\left\{ \frac{1}{4} \int\limits_{dab} \left(1 + \frac{u(\zeta)}{u(\xi)}\right) \frac{d\xi}{\xi - \zeta} - \frac{1}{2} \int\limits_{\gamma} \left(1 + \frac{u(\zeta)}{u(\xi)}\right) \frac{d\xi}{\xi - \zeta} - \frac{1}{2} \int\limits_{\gamma} \left(1 - \frac{u(\zeta)}{\overline{u(\xi)}}\right) \frac{d\bar{\xi}}{\bar{\xi} - \zeta} - 2n_a \int\limits_{l_0^+} \frac{u(\zeta)}{u(\xi)} \frac{d\xi}{\xi - \zeta} \right\}, \tag{3.43}$$

where γ is a continuous curve whose starting and terminal points are $\boldsymbol{\eta}_0 = (\eta_0, u(\eta_0))$ and $\boldsymbol{\zeta}_0 = (\zeta_0, u(\zeta_0))$, respectively. The point $\boldsymbol{\eta}_0$ is an arbitrary fixed point lying on the upper sheet $\mathbb{C}_1$, whilst the point $\boldsymbol{\zeta}_0$ can lie on either sheet. The affix ζ_0 of the starting point is defined by

$$\zeta_0 = \mathrm{sn}^2 \frac{ig_0}{2k}, \tag{3.44}$$

where

$$k = m^{-1/2}, \quad g_0 = \frac{1}{4} \int\limits_{dab} \frac{d\xi}{p^{1/2}(\xi)} + \int\limits_0^{\eta_0} \frac{d\xi}{p^{1/2}(\xi)}. \tag{3.45}$$

Denote

$$I_\pm = \frac{1}{4} \int\limits_{dab} \frac{d\xi}{p^{1/2}(\xi)} + \int\limits_0^{\eta_0} \frac{d\xi}{p^{1/2}(\xi)} \pm \int\limits_0^{\zeta_0} \frac{d\xi}{p^{1/2}(\xi)}. \tag{3.46}$$

If it turns out that both the numbers

$$-\frac{\operatorname{Im} I_-}{4k\mathbf{K}} \quad \text{and} \quad \frac{\operatorname{Re} I_-}{4k\mathbf{K}'} \tag{3.47}$$

are integers, then the point $\boldsymbol{\zeta}_0 \in \mathbb{C}_1$ and $n_a = -\operatorname{Im} I_-(4k\mathbf{K})^{-1}$. Otherwise, the point $\boldsymbol{\zeta}_0$ falls on the lower sheet $\mathbb{C}_2$ and $n_a = -\operatorname{Im} I_+(4k\mathbf{K})^{-1}$. Here $\mathbf{K} = \mathbf{K}(k)$ is the complete elliptic integral of the first kind, and $\mathbf{K}' = \mathbf{K}(\sqrt{1-k^2})$.

The curve γ does not cross the contour l_0. In the case $\boldsymbol{\zeta}_0 \in \mathbb{C}_2$, it passes through the point $\zeta = 0$ and consists of two parts, $\boldsymbol{\eta}_0\,\mathbf{0} \subset \mathbb{C}_1$ and $\mathbf{0}\,\boldsymbol{\zeta}_0 \subset \mathbb{C}_2$. If the point $\boldsymbol{\zeta}_0$ lies on the upper sheet, then the contour γ can be chosen as the straight line joining the points $\boldsymbol{\eta}_0$ and $\boldsymbol{\zeta}_0$ provided it does not cross the contour l_0. We notice that in all the numerical tests implemented the point $\boldsymbol{\zeta}_0 \in \mathbb{C}_1$.

The solution (3.39) possesses 10 unknown real constants. They are M_0, M_1, M_2, and M_3 (the coefficients in the representation of the rational function $\Omega(\zeta, u)$), the angle of yaw δ, and the points a, b, d, e_0, and m. To fix these unknowns we have the same number of equations, linear and nonlinear. The first equation (3.36) links the three parameters a, e_0, and m. Write down the other equations. Due to the simple pole of the function $X(\zeta, u)$ at the point $\boldsymbol{\zeta}_0$, the function $\omega_1(\zeta)$ has an inadmissible pole at this point. It becomes a removable singularity if the following complex condition holds

$$\Psi(\zeta_0, u(\zeta_0)) + \Omega(\zeta_0, u(\zeta_0)) = 0. \tag{3.48}$$

To guarantee a smooth detachment of the jet breaking away from the wedge at the point $z = D$, we require

$$\Psi(d, u(d)) + \Omega(d, u(d)) = 0. \tag{3.49}$$

Notice that at the point $\zeta = b$ the solution is automatically bounded.

Since the function $\omega_1(\zeta)$ vanishes at the point $\zeta = e_1$, we impose the following condition

$$\Psi(e_1, u(e_1)) + \Omega(e_1, u(e_1)) = 0. \tag{3.50}$$

Next, we wish the function $\omega_1(\zeta)$ being bounded at the infinite point. By analyzing the principal term in (3.39) at infinity, we have

$$M_0 = \Psi_0 - 2M_2, \tag{3.51}$$

where Ψ_0 is a real constant given by

$$\Psi_0 = \frac{\alpha}{2\pi}\int\limits_{ab}\frac{d\xi}{vX^+(\xi, v)} - \frac{\pi-\beta}{2\pi}\int\limits_{da}\frac{d\xi}{vX^+(\xi, v)}$$

$$+\frac{i\ln(\sigma+1)}{4\pi}\int\limits_{bcd}\frac{d\xi}{vX(\xi, v)}. \tag{3.52}$$

We also add the standard geometrical conditions

$$\lambda_1^\circ \sin\alpha - \Omega_1 = 0, \quad \lambda_2^\circ \sin\beta - \Omega_2 = 0, \tag{3.53}$$

where

$$\Omega_1 = \operatorname{Im}\int\limits_{ab}\omega_0^*(\zeta)e^{-\omega_1(\zeta)}d\zeta,$$

$$\Omega_2 = \operatorname{Im}\int\limits_{da}\omega_0^*(\zeta)e^{-\omega_1(\zeta)}d\zeta. \tag{3.54}$$

The final two real equations come from the requirement for the mapping $z = f(\zeta)$ to satisfy the single-valuedness condition (3.32) or, equivalently, the following condition

$$\int\limits_{l_1^*}\omega_0^*(\zeta)e^{-\omega_1(\zeta)}d\zeta = 0, \tag{3.55}$$

where l_1^* is a closed contour around the cut l_1 which does not cross the cut l_0.

The real constants $M_0, \ldots, M_3$ and the angle of yaw $\delta = \alpha - \alpha_0$ are determined explicitly from the linear equations (3.48) to (3.51). The other

unknown parameters of the conformal mapping, a, b, d, e_1, and m, can be found from a system of three real and one complex transcendental equations (3.36), (3.53), and (3.55).

The nonlinear system (3.36), (3.53), and (3.55) of five real equations is solved numerically by a technique based on the Newton method similarly to the system of four nonlinear equations associated with the problem for a wedge beneath a free surface [4]. The main feature of the system (3.36), (3.53), and (3.55) is the presence of certain constraints for the unknown parameters. Indeed, we have chosen $a \in l_1^+$, have proved that $c = \bar{a} \in l_1^-$, and $1 < m < \infty$ by the definition. Therefore, $d \in l_1^{\pm}$, $b \in l_1^{\pm}$ and $0 < d < a$, $a < b < 1$. All numerical tests implemented show that in fact, $d \in l_1^+$ and $b \in l_1^+$. It turns out that there are two sets of parameters of the conformal mapping, $\{a, b, d, e_1, m\}$ and $\{a, b, d, \bar{e}_1, m\}$, which satisfy the system of nonlinear equations. However, the set of parameters with $e_1 = e_0 - i0$ produces a nonphysical solution: the two branches of the free streamline which define the cavity intersect each other, and the Brillouin condition is therefore violated.

For all the problem parameters tested, the physical solution corresponds to the case when $e_1 = e_0 + i0 \in l_0^+$ and therefore $e_2 = \bar{e}_1 \in l_0^-$. The values of the parameters of the conformal mapping and the angle of yaw for some values of the cavitation number σ when

$$\alpha_0 = \frac{\pi}{3}, \quad \beta_0 = \frac{2\pi}{3}, \quad \lambda_1 = 1, \quad \lambda_2 = 2,$$
$$h = 20, \quad h_1 = 10, \qquad (3.56)$$

are given in Table 1. It is seen that the angle of yaw increases when the cavitation number increases.

Table 1. The values of the parameters a, b, d, e_0, m, and the yaw angle δ for the parameters (3.56) and some values of the cavitation number σ.

σ	a	b	d
0.3	0.991565	0.996192	0.971464
0.6	0.960173	0.982899	0.862127
1.0	0.870908	0.948976	0.570754
σ	e_0	$m-1$	δ
0.3	1.0084579	$1.395441 \cdot 10^{-6}$	0.129164
0.6	1.043103	$1.561740 \cdot 10^{-3}$	0.134618
1.0	1.170520	$1.958512 \cdot 10^{-2}$	0.141443

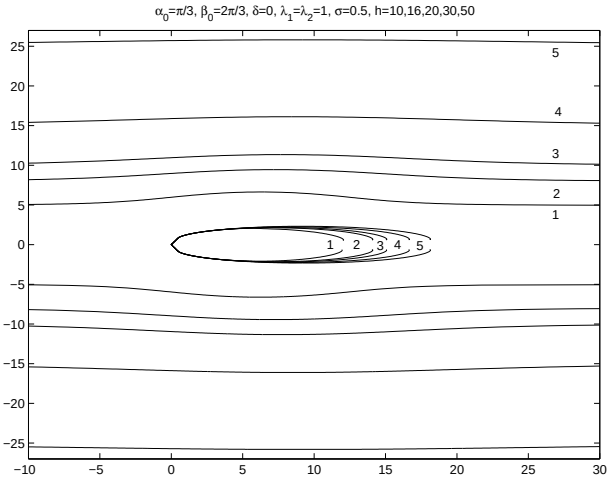

Figure 5: The cavity shape and the jet surface when $\alpha_0 = \pi - \beta_0 = \frac{\pi}{3}$, $\lambda_1 = \lambda_2 = 1$, $l = 0.5$, $\sigma = 0.5$ for some values of the h: $h = 10$ (1), $h = 16$ (2), $h = 20$ (3), $h = 30$ (4), and $h = 50$ (5).

To restore the shape of the cavity, we integrate the function $df/d\zeta$ over the contours $b\tau$ ($\tau \in bc$) and $d\tau$ ($\tau \in dc$) as was described in the case of the double-spiral-vortex model in Section 2.3. We have reconstructed the shape of the cavity behind the wedge and the jet for a symmetric wedge for different widths h of the jet or equivalently for different values of the parameter $\lambda_1^\circ = \lambda_2^\circ$ (figure 5). The numerical results show

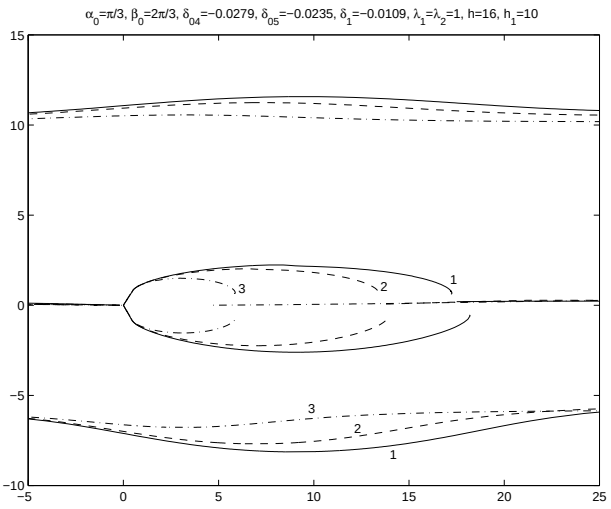

Figure 6: The cavity shape and the jet surface for $\alpha_0 = \pi - \beta_0 = \frac{\pi}{3}$, $\lambda_1 = \lambda_2 = 1$, $l = \frac{5}{8}$ when $\sigma = 0.4$ (1), $\sigma = 0.5$ (2), and $\sigma = 1$ (3).

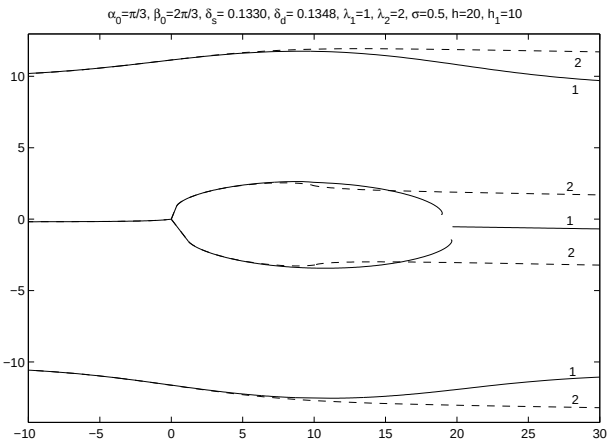

Figure 7: The cavity shape and the free surface for a nonsymmetric wedge when $\alpha_0 = \frac{\pi}{3}$, $\beta_0 = \frac{2\pi}{3}$, $\sigma = 0.5$, $h = 20$, $h_1 = 10$, $\lambda_1 = 1$, and $\lambda_2 = 2$ for the single- (1) and double-spiral-vortex (2) models.

that when h grows and the cavitation number is fixed the length of the cavity grows as well.

The jet boundary, the cavity shape and the streamline which splits at the vertex of the wedge and then emerges at the rear part of the cavity are shown in figure 6 for some cavitation numbers in the nonsymmetric case. The amplitude of the wave on the surface of the jet and the cavity length increase when the cavitation number decreases.

In figure 7, we present the cavity and jet profiles predicted according to the single-spiral-vortex model (a solid line) and the double-spiral-vortex model (a broken line). In the contrast to the second model, there is no wake behind the cavity in the former model. The shapes of the cavity computed according to the two models, are different only at the rear part of the cavity. The length of the cavity is smaller for the double model, however the separation point between the cavity and the wake is hardly noticeable. Also, the jet is wider for the double model. This is again because of the presence of the wake behind the cavity.

The solid lines in figure 3 correspond to the drag and lift coefficients C_X and C_Y computed in the framework of the single-spiral-vortex model. It is seen that the curves for the single- and double-spiral-vortex model (the broken lines) are very close to each other. In the nonsymmetric case, as $x_1 \to +\infty$, the speed $V \to V_\infty$. The velocity vector $\mathbf{v}$ however does not tend to $(V_\infty, 0)$. This is because of the jet deflexion. In Table 2, we give some values of the angle of deflection ϵ at infinity for both the models. It is small and of the same order for both the models.

Table 2. The angle of deflection ϵ for the single-spiral-vortex model (SSVM) and the double-spiral-vortex model (DSVM) of the jet at infinity for $\alpha_0 = \pi - \beta_0 = \pi/3$, $\lambda_1 = 1$, $\lambda_2 = 2$, $h = 20$, $h_1 = 10$.

σ	SSVM	DSVM
0.3	-0.01524	-0.01661
0.5	-0.02294	-0.01811
0.7	-0.02745	-0.01954
1.0	-0.03392	-0.02160

Finally, we determine the circulation of the velocity around the closed contour $L_1 = ABCDA$ for the single-spiral-vortex model

$$\Gamma = \int\limits_{l_1^*} \frac{dw}{d\zeta} d\zeta = hV_\infty \int\limits_{l_1^*} \tilde{\omega}_0(\zeta) d\zeta. \qquad (3.57)$$

Table 3. Circulation $(V_\infty)^{-1}\Gamma$ for the single-spiral-vortex model: $\alpha_0 = \pi/3$, $\beta_0 = 2\pi/3$, $\lambda_1 = 1$, $\lambda_2 = 2$, $h = 20$, $h_1 = 10$.

σ	$(V_\infty)^{-1}\Gamma$
0.3	-10.454608
0.4	-5.668399
0.6	-1.094609
1.0	-0.792022

It is seen from Table 3 that for a nonsymmetric wedge, the absolute values of the circulation, $|\Gamma|$, decreases when the cavitation number σ increases. As h increases and h_1 is fixed, Γ/V_∞ decreases: for $h_1 = 10$, $\lambda_1 = \lambda_2 = 1$, $\sigma = 0.5$, $\alpha_0 = \pi - \beta_0 = \pi/3$ and for $h = 30, 80$, and 150 we have $\Gamma/V_\infty = -0.4845$, -0.3520 and -0.3288, respectively that is consistent with the results [4] for a wedge beneath a free surface. Because of the condition (2.5), the corresponding integral around the contour C_1DABC_2 for the double-spiral-vortex model is zero.

4 Two wedges in a jet

Consider the single-spiral-vortex model for two supercavitating wedges symmetrically located with respect to the line of symmetry E_1E_2 for

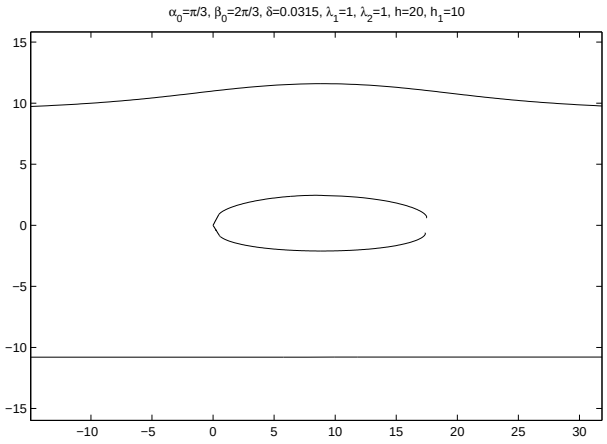

Figure 8: The cavity shape and the free surface for a wedge in a channel (two symmetric wedges in a jet) when $\alpha_0 = \frac{\pi}{3}$, $\beta_0 = \frac{2\pi}{3}$, $\sigma = 0.3$, $h = 5$, and $\lambda_1 = \lambda_2 = 1$, $h = 20$ and $h_1 = 10$.

the jet of width $2h$ when it is calm. This problem is equivalent to the problem for a wedge in a channel with a free surface $E_1^+E_2^+$. The lower boundary is rigid and therefore, $\arg\frac{dw}{dz} = 0$, $z \in E_1E_2$. The problem can be solved similarly to the case of one wedge in a jet by using the conformal map $z = f(\zeta)$ whose derivative has the form (2.7) with the function $\omega_0(\zeta)$ defined in (3.34). The second function, $\omega_1(\zeta)$, in addition to the boundary condition (3.37) has to meet the condition $\mathrm{Im}\,\omega_1(\zeta) = 0$, $\zeta \in e_1e_2$. In comparison to the case of one wedge in a jet, the only one difference in the representation of the function $\omega_1(\zeta)$ is the contour of integration in the first integral in formula (3.43) for the function $X(\zeta, u)$: the contour dab is to be replaced by $dab \cup e_1e_2$. The final solution has the same number of unknown parameter and the same number of additional conditions. Note that to fix the position of the wedge in the channel, we use the condition (3.35), where h_1 is the parameter introduced in

Section 2.

In figure 8, we show the predicted shape of the cavity and the upper free surface. It is seen that the presence of the bottom or, equivalently, another symmetrically located wedge turns the wedge (the yaw angle for the parameters chosen is 0.0315).

Conclusions

The main contribution of this work is the comparative analysis of the two nonlinear models by Tulin, the single- and double-spiral-vortex models applied to the problem for a jet past a yawed nonsymmetric wedge.

By solving certain Riemann-Hilbert problems we have derived the conformal mapping from a parametric half-plane onto the flow domain for the double-spiral-vortex model and from a plane cut along two segments, $[0, 1]$ and $[m, \infty)$, onto the physical domain for the single-spiral-vortex model. The former case is simpler since the Riemann-Hilbert problem is set on the complex plane whilst it is formulated on a genus-1 Riemann surface in the case of the single-spiral-vortex model. In both the models, the final step of the method is the solution of an associated system of transcendental equations for the unknown parameters of the conformal mapping. We have solved these systems by the Newton type method. It turns out that the nonlinear system in the double-spiral-vortex model has a unique solution. For the single-spiral-vortex model, we have found two sets of parameters. However, one of them violates the Brillouin condition which requires the free streamlines do not intersect each other. The second solution obeys all the conditions of the model and is therefore physical.

The numerical results for the drag and lift coefficients computed according to the single- and double-spiral-vortex models are very close. What is different is the shape of the rear part of the cavity, its length, and also the profile of the jet. In general, the amplitude of the waves on the jet are higher in the double-spiral-vortex model. After the jet hits the wedge it deflects from the original horizontal axis. Again, the deflection angles computed at infinity are not the same for the two models. Finally, in general, the circulation is not zero for the single-spiral-vortex model while it always vanishes in the double-spiral-vortex model.

Acknowledgments. This work was funded by NSF through grant DMS0707724.

References

[1] Antipov, Y.A. & Silvestrov, V.V. 2007 Method of Riemann surfaces in the study of supercavitating flow around two hydrofoils in a channel. *Physica D* **235**, 72-81.

[2] Antipov, Y.A. & Silvestrov, V.V. 2008 Double cavity flow past a wedge. *Proc. R. Soc. A* **464**, 3021-3038.

[3] Antipov, Y.A. & Silvestrov, V.V. 2009 Circular map for supercavitating flow in a multiply connected domain. *Quart. J. Mech. Appl. Math.* **62**, 167-200.

[4] Antipov, Y.A. & Zemlyanova, A.Y. 2009 Motion of a yawed supercavitating wedge beneath a free surface. *SIAM J. Appl. Math.* to appear.

[5] Bassanini, P. & Elcrat, A. 1988 A univalent spiral-vortex model for separated flow past a polygonal obstacle. *ZAMP* **39**, 455-467.

[6] Brennen, C.E. 1985 *Cavitation and Bubble Dynamics*, Oxford, UK: Oxford University Press.

[7] Furuya, O. 1975 Nonlinear calculation of arbitrary shaped supercavitating hydrofoils near a free surface. *J. Fluid Mech.* **68**, 21-40.

[8] Gilbarg, D. 1960 *Jets and cavities*, Handbuch der Physic, **9**, 311-445, Berlin, Germany: Springer-Verlag.

[9] Gurevich, M.I. 1979 *The Theory of Jets in an Ideal Fluid*. Moscow, Russia: Nauka.

[10] Larock, B. & Street, R. 1967 Nonlinear solution for a fully cavitating hydrofoil beneath a free surface, *J. Ship Res.* **11**, 131-140.

[11] Larock, B. & Street, R. 1975 A Riemann-Hilbert problem for nonlinear, fully cavitating flow, *J. Ship Res.* **9**, 170-178.

[12] Terent'ev, A.G. 1976 Non-linear theory of cavitational flow around obstacles, *Fluid Dynamics* **11**, 142-145.

[13] Tulin, M.P. 1964 Supercavitating flows – small perturbation theory. *J. Ship Res.* **7**, 16-37.

[14] Wu, T.Y. 1972 Cavity and wake flows. *Annu. Rev. Fluid Mech.* **4**, 243-284.